ADVANCED MATERIALS
www.advmat.de

# Temperature Dependence of Relativistic Valence Band Splitting Induced by an Altermagnetic Phase Transition

*Mahdi Hajlaoui,* Sunil Wilfred D'Souza, Libor Šmejkal, Dominik Kriegner, Gauthier Krizman, Tetiana Zakusylo, Natalia Olszowska, Ondřej Caha, Jan Michalička, Jaime Sánchez-Barriga, Alberto Marmodoro, Karel Výborný, Arthur Ernst, Mirko Cinchetti, Jan Minar, Tomas Jungwirth, and Gunther Springholz**

**Altermagnetic (AM) materials exhibit non-relativistic, momentum-dependent spin-split states, ushering in new opportunities for spin electronic devices. While the characteristics of spin-splitting are documented within the framework of the non-relativistic spin group symmetry, there is limited exploration of the inclusion of relativistic symmetry and its impact on the emergence of a novel spin-splitting in the band structure. This study delves into the intricate relativistic electronic structure of an AM material, $\alpha$−MnTe. Employing temperature-dependent angle-resolved photoelectron spectroscopy across the AM phase transition, the emergence of a relativistic valence band splitting concurrent with the establishment of magnetic order is elucidated. This discovery is validated through disordered local moment calculations, modeling the influence of magnetic order on the electronic structure and confirming the magnetic origin of the observed splitting. The temperature-dependent splitting is ascribed to the advent of relativistic spin-splitting resulting from the strengthening of AM order in $\alpha$−MnTe as the temperature decreases. This sheds light on a previously unexplored facet of this intriguing material.**

## 1. Introduction

Exploring the unique properties of electron spins and tailoring their spin splitting holds significant potential for the development of more efficient and versatile spin-electronic devices.[1–5] In conventional antiferromagnets with antiparallel magnetic order, symmetries usually prevent a spin splitting of bands.[6] For this reason, materials where those symmetries are broken have been considered.[7–11] This led to the recent theoretical breakthrough that allowed to identify a new class of materials termed "altermagnets" (AMs)[12] which are distinct from conventional (collinear) antiferromagnets and exhibit a momentum-dependent spin splitting despite the compensation of magnetic moments. The spin splitting in AMs can be of non-relativistic origin, displaying energy splitting orders of magnitude larger than those typically induced by relativistic spin-orbit coupling (SOC). The direction of the spin polarization alternates throughout the Brillouin zone, changing sign upon crossing symmetry-enforced nodal surfaces where spin degeneracy in the non-relativistic electronic structure is maintained. Altermagnetic crystals can exhibit two, four, or six spin-degenerate nodal surfaces, corresponding to d-wave, g-wave, or i-wave type of the non-relativistic spin-polarization order, respectively.[6,12] Here, we focus on $\alpha$−MnTe,

M. Hajlaoui, G. Krizman, T. Zakusylo, G. Springholz
Institute of Semiconductors and Solid-State Physics
Johannes Kepler University
Linz 4040, Austria
E-mail: mahdi.hajlaoui@jku.at; gunther.springholz@jku.at

S. Wilfred D'Souza, A. Marmodoro, J. Minar
University of West Bohemia
New Technologies Research Center
Pilsen 30100, Czech Republic

L. Šmejkal, D. Kriegner, A. Marmodoro, K. Výborný, T. Jungwirth
Institute of Physics
Czech Academy of Sciences
Cukrovarnická 10, Praha 16200, Czech Republic



**DOI: 10.1002/adma.202314076**

L. Šmejkal
Institute of Physics
Johannes Gutenberg University Mainz
D-55099 Mainz, Germany

N. Olszowska
National Synchrotron Radiation Centre SOLARIS
Jagiellonian University
Czerwone Maki 98, Krakow 30-392, Poland

O. Caha
Department of Condensed Matter Physics
Masaryk University
Kotlářská 267/2, Brno 61137, Czech Republic

J. Michalička
Central European Institute of Technology
Brno University of Technology
Purkyňova 123, Brno 61200, Czech Republic

J. Sánchez-Barriga
Helmholtz-Zentrum Berlin für Materialien und Energie
Albert-Einstein-Strasse 15, 12489 Berlin, Germany

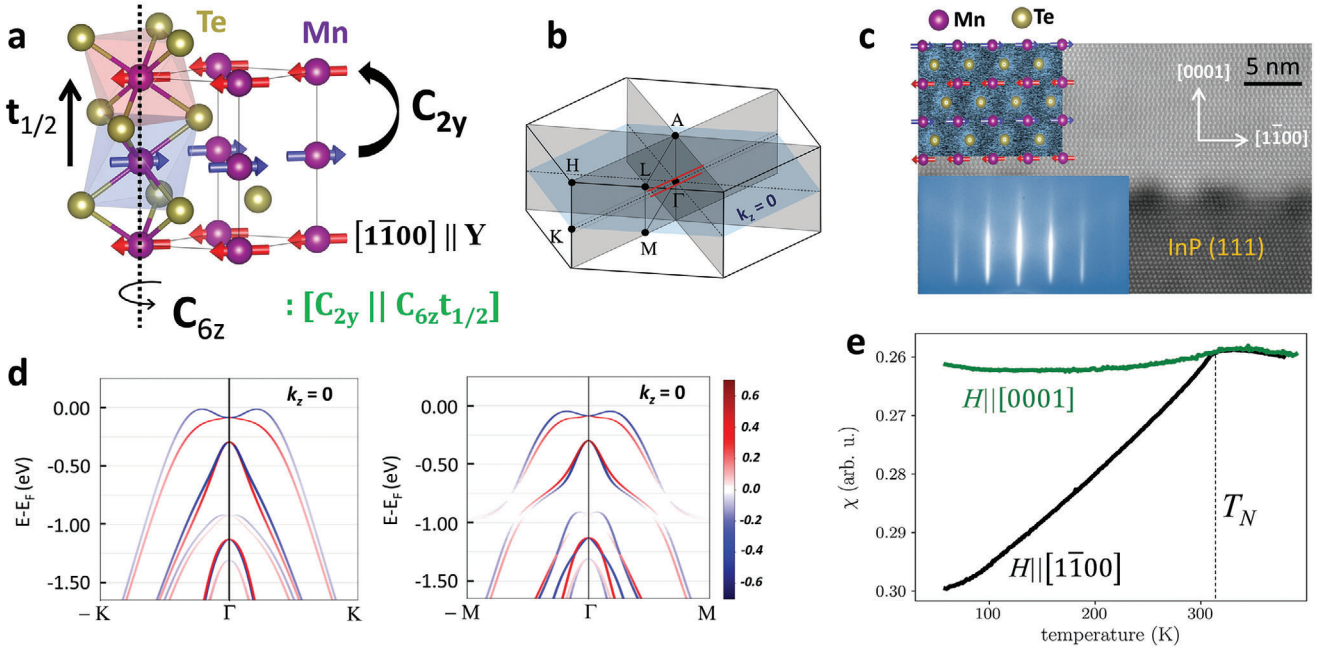


**Figure 1.** Properties of altermagnetic $\alpha$−MnTe. a) AM structure of $\alpha$-MnTe with opposing spin-sublattices connected by a non-symmorphic sixfold screw-axis rotation $C_{6z}t_{1/2}$ combined with $C_{2y}$ spin rotation: $[C_{2y} \parallel C_{6z}t_{1/2}]$. The Néel vector is oriented along the $[1\bar{1}00]$ direction. b) Bulk Brillouin zone, displaying the four nodal degenerate surfaces (grey and blue planes). The two red lines delineate the cuts in k-space on the nodal surfaces (AHKΓ) where temperature-dependent ARPES is conducted at $h\nu = 21$ and 48 eV (see Figure 3). c) HAADF-STEM image along the $[11\bar{2}0]$ direction. A corrugation of approximately five atomic layers is observed at the MnTe/InP(111) interface, which is attributed to the high-temperature annealing necessary to remove the native oxide of the InP surface. A zoomed view of the MnTe epilayer is displayed in the upper left corner, while the lower left inset presents in situ RHEED patterns recorded at the MnTe (0001) surface during MBE growth. d) The electronic structure of AM-MnTe along the Γ−K and Γ−M directions with spin-orbit coupling, highlighting the spin-polarized states at the $k_z = 0$ plane, with red and blue colors representing spin up and spin down, respectively. e) Temperature-dependent susceptibility measured under different magnetic field directions.

identified as a g-wave altermagnet in the absence of SOC.[6,12] We delve into the implications of the relativistic SOC in the AM-MnTe in inducing additional relativistic spin splitting on these nodal surfaces.

$\alpha$−MnTe crystallizes in the hexagonal NiAs- structure with a space group symmetry of $P6_3/mmc$ (see **Figure 1a**). In the magnetically ordered phase, the Mn moments align parallel within each c-plane but stack antiparallel along the $c$–axis, resulting in a collinear magnetically compensated phase. Without SOC, the spin sublattices are connected by a non-symmorphic sixfold screw-axis rotation $C_{6z}t_{1/2}$ combined with $C_{2y}$ spin rotation: $[C_{2y}||C_{6z}t_{1/2}]$. The resulting non-relativistic spin-group symmetry ($^2$6/$^2$m$^2$m$^1$m) reveals a strong time-reversal symmetry breaking and alternating spin splitting in the band structure.[6,12,13] Consequently, $\alpha$−MnTe falls into the g-wave AM category, characterized by three spin-degenerate nodal planes crossing the Γ−point and parallel to the $c$–axis (grey planes in Figure 1b), and one more spin-degenerate nodal plane crossing the Γ−point orthogonal to the $c$–axis (the $k_z = 0$ plane; the blue plane in Figure 1b). When SOC interaction is introduced, the relativistic magnetic point group varies depending on the Néel vector orientation.[13] By inclusion of SOC in the AM symmetry, the spin degeneracy within these nodal planes is lifted. This effect is illustrated in Figure 1d for the case of $k_z = 0$ plane, along the Γ−K and Γ−M directions, depicting the spin-polarized band structure, with red and blue colors representing spin up and spin down, respectively.[14]

The experimental exploration of AM properties of $\alpha$−MnTe has started with the observation of the spontaneous anomalous Hall effect[13,15] serving as a signature rather than direct evidence for AM. Angle-resolved photoemission spectroscopy (ARPES) thus, plays a pivotal role in investigating the altermagnetism of $\alpha$−MnTe.[14,16,17] Soft X-ray ARPES and Spin-ARPES have been recently employed to measure the bulk and spin polarized electronic structure, providing the first experimental evidence of AM lifting of Kramer's spin degeneracy.[14] In addition, ARPES along $k$-space directions not aligned with nodal surfaces was used to measure the energy splitting induced by the AM phase

J. Sánchez-Barriga
IMDEA Nanoscience
C/Faraday 9, Campus de Cantoblanco, Madrid 28049, Spain
A. Ernst
Institute for Theoretical Physics
Johannes Kepler University
Linz 4040, Austria
M. Cinchetti
Department of Physics
TU Dortmund University
44227 Dortmund, Germany
T. Jungwirth
School of Physics and Astronomy
University of Nottingham
Nottingham NG7 2RD, UK

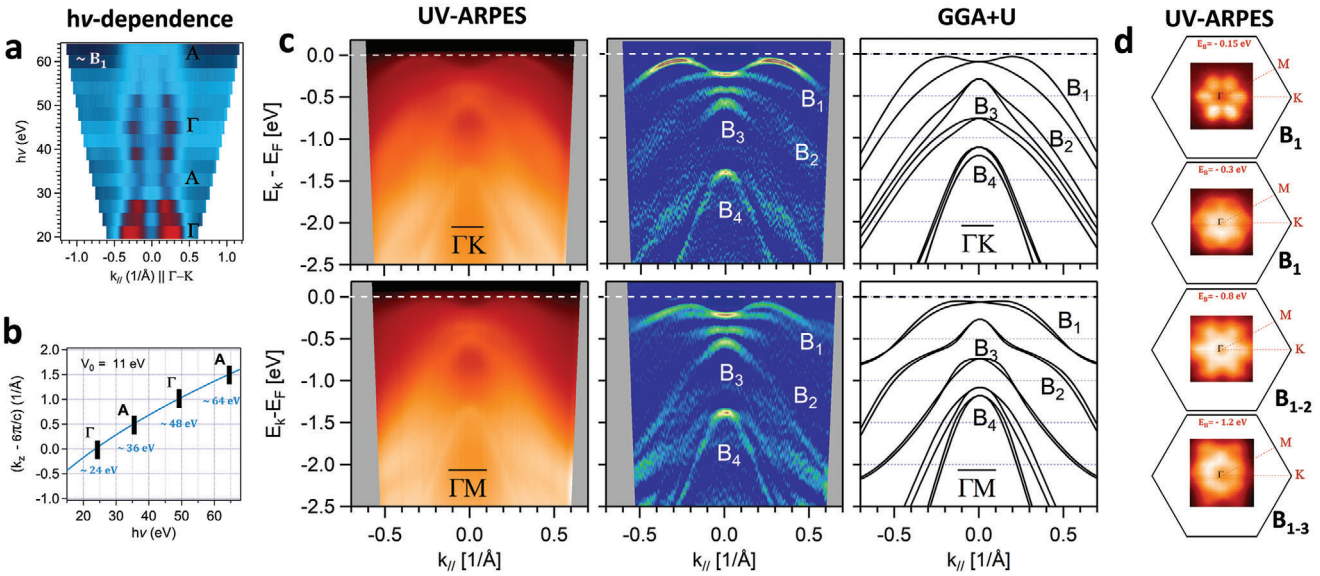


**Figure 2.** The relativistic electronic structure of $\alpha$−MnTe: a) Photon energy dependence of UV-ARPES integrated over the bulk $B_1$ band near the Fermi level at $T = 40$ K (AM-phase). Here, the red color corresponds to the highest intensity. b) The $k_z$ values as a function of photon energy at normal emission and near the Fermi level, assuming a parabolic final state of bands and an inner potential of $V_0 = 11$ eV. The positions of Γ and A are indicated. c) UV-ARPES $E(k_{||})$ band maps (left) and their second derivative in blue (middle) recorded at $h\nu = 21$ eV at 40 K along the Γ−K (top) and Γ−M directions (bottom). The corresponding bulk GGA+$U$ calculations are shown on the right, showcasing the emergence of three groups of bulk bands $B_1$, $B_2$, $B_3$ each consisting of two spin split bands, and group $B_4$ consisting of four split bands. d) Constant energy cuts of the UV-ARPES data mapped to the ($k_x$, $k_y$) plane at different energies of −0.15, −0.3, −0.8, and −1.2 eV below the Fermi level.

transition[16] and micro-focused ARPES on a single crystal provided insights into the anisotropic spin-split band structure of the AM phase.[17] The application of ARPES also identified the AM properties in other prototypical materials, such as $RuO_2$[18] and CrSb.[19]

In the present work, we present temperature-dependent UV-ARPES measurements spanning over the whole magnetic phase transition, with particular attention directed toward states on the nodal surfaces. The results unveil a temperature-dependent relativistic spin splitting that diminishes gradually as the system approaches the paramagnetic (PM) phase. Through the utilization of disordered local moment (DLM) calculations to model the PM-AM transition, we demonstrate the magnetic origin of the AM valence band splitting. The microscopic rationale for this magnetism-induced splitting lies in the establishment of the relativistic AM symmetry as the temperature decreases below the Néel temperature. This sheds light on an important unexplored facet of this intriguing class of materials.

## 2. Results and Discussion

For our investigations, single crystalline $\alpha$−MnTe films were grown on InP (111) substrates using molecular beam epitaxy, as detailed in the Experimental Section. Under optimized conditions, we obtained high-quality epitaxial layers with hexagonal NiAs-type structure in the (0001) orientation and excellent surface properties. The characterization of the film was carried out using high-angle annular dark-field scanning transmission electron microscopy (HAADF-STEM) and reflection high-energy electron diffraction (RHEED), as shown in Figure 1c. X-ray diffraction (XRD) and atomic force microscopy (AFM) were also employed, yielding consistent results with our previous works.[20–23] For further insights into the magnetic transition, we conducted temperature-dependent susceptibility measurements under various magnetic field directions, revealing an AM phase transition at $T_N = 307$ K (see Figure 1e). For UV-ARPES investigations, the films were transferred from our molecular beam epitaxy system to the U125-2-PGM and URANOS beamlines at SOLARIS and BESSY II synchrotron facilities without breaking the ultra-high vacuum conditions ($<10^{-10}$ mbar).

### 2.1. The Relativistic Altermagnetic Electronic Structure

To reveal the electronic band structure of the AM phase, we first focus on the ARPES photon energy dependence at $T = 40$ K to elucidate the dispersion of the band structure along the $k_z$-direction and thereby, determine the positions of the high symmetry points Γ and A as a function of photon energy in the range of 19 to 65 eV. Pure surface states typically do not disperse with photon energy, whereas surface resonances and bulk projected bands usually significantly disperse along the $k_z$ direction. **Figure** 2a presents integrated photon energy-dependent ARPES spectra within an energy window of 50 meV, centered at a binding energy of 150 meV below the Fermi level. This exclusive focus reveals the dispersion of states corresponding to band $B_1$. The results indicate a distinct $k_z$-dispersion of $B_1$ across different photon energies. A periodic pattern in the dispersion is noticeable, particularly around $h\nu = 22$ and 46 eV, where a broader $k_{||}$ momentum dispersion is observed. Conversely, at $h\nu = 36$ and 64 eV, the map illustrates dispersion within a narrower $k_{||}$ range. The Γ and A points have been attributed to these photon energies, respectively. This

is supported by Figure 2b, showing the positions of Γ and A in $k_z$ values, assuming a parabolic final state with an inner potential $V_0 = 11$ eV. The same inner potential was also used to calculate the $k_z$-dependence of the soft-X-ray ARPES data, revealing a consistent dispersion as in one-step photoemission calculations.[14] This observation suggests that $B_1$ may exhibit characteristic features indicative of its bulk nature. We would like to note that because the data in Figure 2a shows the $k_z$ dispersion at 100 – 200 meV below the Fermi level, it does not indicate the position of the valence band maximum, as discussed in Ref. [24].

For further analysis, we show in Figure 2c the $E(k_{||})$ ARPES maps recorded at 21 eV close to the Γ−point, along the two high-symmetry $k_{||}$-directions Γ−K (top) and Γ−M (bottom), respectively. For better visualization, the second derivative of these maps is shown in the middle panels to highlight the individual band dispersions. Evidently, the band $B_1$ splits up in two branches away from the Γ-point with a nearly quadratic increase of the splitting with increasing $k_{||}$, which is more pronounced in the Γ−K compared to the Γ−M direction. This unique feature is attributed to the spin splitting of the AM bands shown in Figure 1d, and it perfectly agrees with the bulk GGA+$U$ (GGA; generalized gradient approximation) calculations including SOC shown on the right-hand side of Figure 2c. The importance of including SOC is shown in Note S1, Supporting Information, which presents the comparison of the ARPES data with the GGA+$U$ without SOC, clearly evidencing the spin splitting due to the relativistic effect in the electronic structure.

The temperature-dependent measurements presented below provide additional clarity, reinforcing that the observed energy splitting is a result of spin splitting induced by the AM order. The comparison with the GGA+$U$ calculation reveals that in ARPES, we consistently observe the energy-momentum dispersions for all bands $B_1$, $B_2$, $B_3$, and $B_4$, confirming their dominant bulk character. This is elucidated further in the next section through a comparison of the temperature dependence of these bands and DLM calculations that model the PM-AM transition.

It is important to consider the effect of SOC in the presence of the magnetic order. In fact, as outlined in Note S2, Supporting Information and detailed in Refs. [24,25] the combination of an in-plane Néel vector and SOC interaction breaks the in-plane sixfold symmetry of the electronic structure.[26] In real materials, however, the magnetic structure will form domains with different orientations of the Néel vector along one of the six equivalent in-plane easy axes.[20,21,27] The size of these domains typically varies strongly as a function of temperature and sample growth conditions, but is expected to be well below the spot size of our UV-ARPES measurements (>100 µm). As a result, in our measurements we average the band structure over multiple domains. This averages out the anisotropy as is demonstrated in Figure 2d by the constant energy cuts of the ARPES data, which display a perfect hexagonal symmetry of the band maps for all energies below the Fermi level, with no discernible evidence of anisotropy or the presence of twofold symmetry. Unlike the works of Ref. [16] which lacked information on the anisotropic electronic structure in the presence of SOC, our present density functional theory (DFT) and ARPES data detail this effect and demonstrate an isotropic electronic structure due to the presence of multiple magnetic domains. As shown in Note S2 and Figure S3, Supporting Information, fortuitously, the band structure varies only slightly from one domain to another, so that the main features of the bands—namely their splitting, remain well visible in our experiments even when multiple domains are superimposed. As a result, the large relativistic AM splitting of the band $B_1$ is well visible in our ARPES maps even after the averaging process.

### 2.2. Spin Splitting Induced by the Altermagnetic Phase Transition

To elucidate the influence of AM order on the lifting of spin degeneracy during the magnetic phase transition, we systematically studied temperature-dependent ARPES from 50 K (below $T_N$) to 320 K (above $T_N$). **Figure 3a** presents the resulting ARPES data (first derivative) acquired at $h\nu = 21$ eV along Γ−K, revealing a strong temperature evolution of the band structure. Similar data was measured at $h\nu = 48$ eV as depicted in Figure 3b, where the corresponding $k_z$ value lies also in close proximity to Γ (refer to Figure 2a,b). At both 21 and 48 eV the ARPES maps are parallel to the Γ−K direction, as indicated by the respective red cut lines in Figure 1b, capturing the electronic structure on the same nodal surface (AHKΓ, see Figure 1b). The complete raw data and its derivatives are shown in Note S3, Supporting Information. We would note that the prime feature of altermagnets lies in the strong dependence of the spin splitting in different $k$-space directions. Accordingly, the choice of k-space directions along which the temperature-dependent ARPES experiments are performed is of key importance for the assessment of the AM spin splitting. While the temperature dependence in Ref. [16] are measured parallel to Γ−M direction (D-U direction) that is not on the nodal surface, on which the spin splitting can be present even in the case of weak or absent SOC, our focus centers on discerning the spin splitting on the nodal surfaces that require the presence of SOC within the altermagnetic order (see Figure 1d).

Analyzing the ARPES images for $h\nu = 21$ eV (Figure 3a), we clearly find that with increasing temperature the splitting of the $B_1$, $B_2$, and $B_3$ bands gradually diminishes, whereas from 270 K the splitting apparently disappears. Similar features are also observed for the spectra at $h\nu = 48$ eV (Figure 3b). Notably, the drastic change of the splitting is most prominent for bands $B_1$, $B_2$, and $B_3$, while band $B_4$ remains more or less unaffected. Hence, our ARPES measurements at photon energies of 21 and 48 eV demonstrate a temperature-dependent valence band splitting on the nodal surface that is clearly induced by the altermagnetism of the system.

The detailed analysis of the splitting evolution is presented in **Figure 4a**, illustrating the pronounced change in the momentum-integrated energy dispersion curves (EDC) presented as $\Delta\mathrm{EDC}(T) = \mathrm{EDC}(T < 320\ \mathrm{K}) - \mathrm{EDC}\ (320\ \mathrm{K})$, clearly demonstrating the strong increase of the splitting when the temperature is lowered from 270 to 50 K. In particular, the difference spectra clearly reveal the transition from the large splitting of bands $B_1$ and $B_2$ of the low-temperature AM phase to the merged bands in the high-temperature PM phase. Simultaneously, the intensity of the $B_3$ band increases and it shifts to high binding energy. To evaluate the values of temperature-dependent splitting, we focus on the splitting of band $B_1$. We accomplish this by fitting the spectra of $\Delta\mathrm{EDC}(T)$ with two Gaussian curves near these states (depicted as black curves in Figure 4a). The results are presented in Figure 4b, along with the

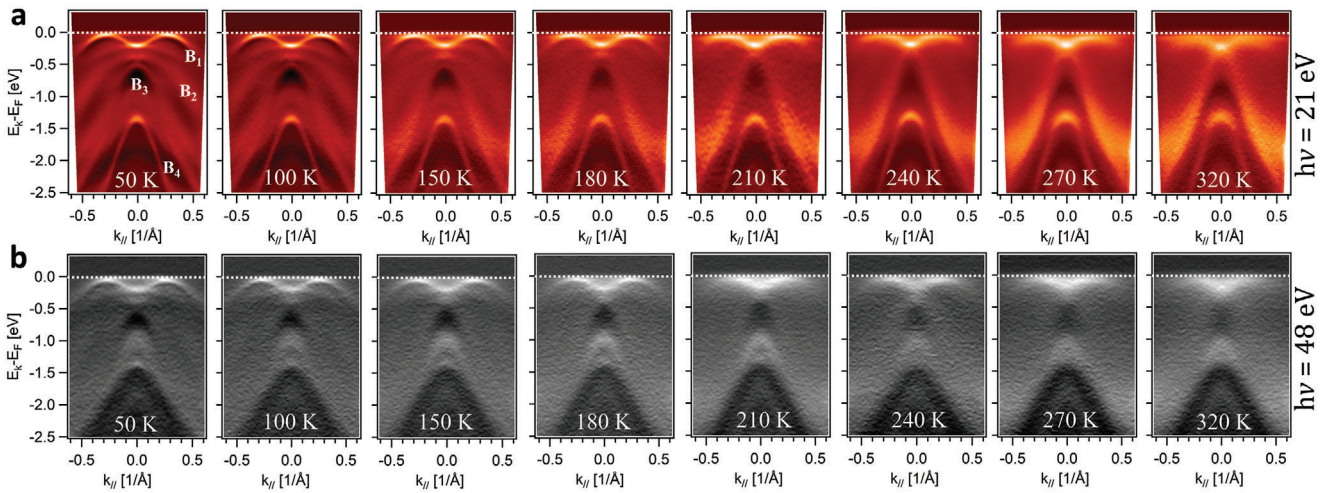


**Figure 3.** Temperature-dependent spin splitting across the AM-PM transition. Temperature-dependent UV-ARPES maps from 50 to 320 K recorded parallel to the Γ−K direction. Data shown in (a) in red was recorded at a photon energy $h\nu = 21$ eV, b) data at $h\nu = 48$ eV is shown in grey scale. The cut lines in *k*-space corresponding to these two-photon energies are highlighted as two red lines in Figure 1b.

temperature-dependent inverse susceptibility from Figure 1e. Evidently, the splitting reaches a maximum value of ≈150 meV at 50 K and gradually decreases until it becomes nearly indiscernible at 270 K. Both the splitting as well as the susceptibility exhibit a similar evolution with temperature, confirming the magnetic origin of the PM-AM transition in $\alpha$−MnTe.

To further corroborate the observed valence band splitting, we compare the low and high-temperature ARPES spectra to band structure calculation using the DLM approach in conjunction with the coherent potential approximation (CPA) to model the electronic structure of both the disordered PM and ordered AM phases (see Experimental Section). The results are displayed in Figure 4c and compared to the ARPES spectra shown in Figure 4d. The calculated band structure shows a remarkably good agreement with the ARPES data both for high-temperature and low-temperature phases, evidencing clearly that the observed

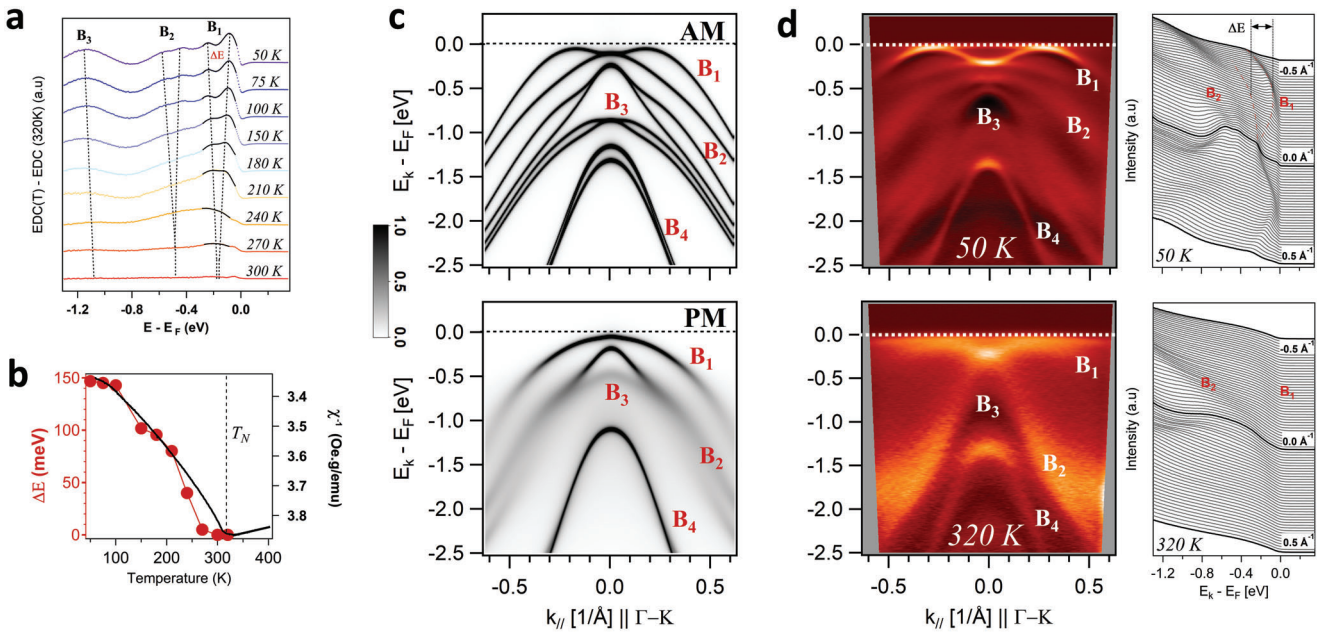


**Figure 4.** Temperature-dependent splitting: ARPES versus DLM-CPA calculations. a) Momentum integrated difference ΔEDC ($T < 320$ K) ARPES profiles minus the EDC at 320 K, that is, ΔEDC($T$) = EDC($T$) − EDC (320 K) as a function of temperature. b) Derived splitting $\Delta E$ of $B_1$ (red symbols) plotted as a function of temperature, alongside the temperature-dependent inverse susceptibility represented by the black line. c) DLM-CPA calculations of the AM (top) and PM (bottom) phases, revealing the pronounced difference in the band structure and spin splitting in the AM and PM states. d) Corresponding UV-ARPES maps at 50 and 320 K below and above $T_N$ along the ΓK direction (first derivative, $h\nu = 21$ eV). The raw data of EDCs at different momenta are shown on the right.

band structure changes are indeed due to the PM-AM phase transition. Specifically, the splitting of bands $B_1$, $B_2$, and $B_3$ is consistently observed in both DLM-CPA and low-temperature ARPES (50 K) but is absent for the high-temperature PM phase, while the $B_4$ band remains nearly unaffected both in theory and experiments. This validates the bulk nature of these bands and affirms that the observed valence band splitting is of magnetic origin. Thus, the influence of the magnetic order on the energy splitting of the electronic structure is well-described by the DLM-CPA model, supporting our observation with ARPES. It is important to note that in the present DLM-CPA calculation, we are using a static $U$ to accommodate the electronic correlations. Although the overall agreement with the experiments is quite convincing with respect to our primary objective to prove that the spin splitting observed for the AM phase is of magnetic origin, describing finer aspects of the band dispersion, particularly for the paramagnetic phase, requires dynamic electronic correlations, which is beyond the scope of the present manuscript.

The microscopic physics underlying the observed temperature-dependent valence band splitting can be attributed to the emergence of relativistic spin splitting resulting from the strengthening of AM symmetry as temperature decreases. As outlined in the introduction, the altermagnetism of $\alpha-$MnTe implies that in the absence of SOC, the spin degeneracy is preserved on the nodal surfaces. Simultaneously, $\alpha-$MnTe is centrosymmetric, meaning that SOC alone cannot induce spin-splitting states. Indeed, our calculations in Figure 1d directly confirm that the unique combination of both SOC and AM order together leads to the emergence of a relativistic spin splitting on the nodal surfaces, emphasizing that the spin splitting on the nodal surfaces is fundamentally relativistic and requires the presence of AM order. Our ARPES spectra, acquired at 21 and 48 eV, capture the states on the nodal surface (cf. Figure 1b). Moreover, our data showcases the strong increase in energy splitting of these states within the electronic structure as the temperature decreases. This observation is attributed to the presence and strengthening of the AM order, a conclusion supported by DLM-CPA calculations. The temperature-dependent ARPES spectra, thus, effectively reveal the impact of altermagnetism-induced spin splitting on the electronic structure manifested through emergent splitting of the valence bands. Thus, it occurs exclusively in the AM phase.

It is noteworthy that the spin-polarized band structure calculations were made under the assumption that the material exists in a single domain. Averaging over the multiple domains, as we do in our ARPES measurements, cancels out the spin polarization unless an unequal domain population is present by growth[14] or applying external magnetic fields. Thus, although our domain-averaged ARPES spectra do not yield information on the spin polarization, yet they effectively unveil the energy splitting of the electronic structure caused by the altermagnetic phase, which is absent in the PM phase. This is revealed in detail in Note S2 and Figure S3, Supporting Information), where it is shown that the energy splitting in the domain averaged band structure indeed retains the prominent band splitting even if the band structure of multiple domains is super-imposed. Consequently, the large splitting of $B_1$ emerging due to the formation of the AM order is well resolved in our experiments. Thus, our observation of the temperature-dependent valence band splitting across the magnetic transition is a clear hallmark of the altermagnetic state of $\alpha-$MnTe.

## 3. Conclusions

Through angle-resolved photoemission spectroscopy and DFT, we have elucidated the electronic structure of altermagnetic $\alpha-$MnTe in both its low-temperature altermagnetic and high-temperature paramagnetic phases. In the altermagnetic phase, we identified a valence band splitting as large as 150 meV on the nodal surface that gradually diminishes as the temperature increases toward the Néel temperature, and ultimately vanishes above in the paramagnetic phase. This discovery strongly supports the notion that the valence band splitting in altermagnets is intricately linked to the unique momentum-dependent spin splitting caused by the altermagnetic order, as confirmed by our DLM calculations. The presence of a temperature-dependent valence band splitting on the nodal surface unequivocally reveals the crucial role of relativistic altermagnetic symmetry in inducing relativistic spin splitting in $\alpha-$MnTe that stands for a prototypical altermagnetic material. Thus, our work not only expands our understanding of altermagnetic phenomena but also opens new avenues for the development of advanced materials with unique electronic properties. As we delve deeper into the intricacies of altermagnetic systems, we anticipate that further discoveries will drive advancements that have profound implications for both fundamental science and technological applications.

## 4. Experimental Section

*Growth and Characterization*: Single crystalline $\alpha-$MnTe films were grown by molecular beam epitaxy on InP (111) A substrates using elemental Mn and Te sources and substrate temperatures in the range of 370 to 450 °C. The structure of the films was determined using X-ray diffraction (XRD) and scanning transmission electron microscopy (STEM) at room temperature. The surfaces were assessed using reflection high-energy electron diffraction (RHEED) and atomic force microscopy (AFM), while the magnetic transition was characterized through superconducting quantum interference device measurements.

*Angle-Resolved Photoemission Spectroscopy*: The measurements were performed at the high-resolution URANOS beamline at SOLARIS synchrotron in Krakow, Poland. Preliminary measurements were also conducted at the U125-2-PGM beamline at BESSY II synchrotron in Berlin. The samples were transferred from the MBE to the synchrotron under UHV conditions using a battery-operated Ferrovac vacuum suitcase. In these experiments, the photon energy was varied within the range of 17 to 70 eV (p-polarized) and the sample temperature between 320 and 40 K. The photoelectrons' kinetic energy and their emission angles were measured by a VG Scienta DA30L electron spectrometer with energy and angular resolution better than 3 meV and 0.1°, respectively.

*Density Functional Calculation + U (DFT+U)*: To compare with ARPES spectra, self-consistent electronic structure calculations were performed for the magnetically ordered phase of $\alpha-$MnTe ($P6_3/mmc$ space group) using the lattice parameters $a = 4.15$ Å and $c = 6.71$ Å. These calculations utilized projector augmented wave pseudopotentials[28] and adopted the implementation of the VASP electronic structure code.[29] The exchange-correlation functional GGA was chosen according to Perdew, Burke, and Ernzerhof.[30] BZ integral were sampled on a $\Gamma-$centered $9 \times 9 \times 4$ mesh, and a consistent energy cutoff of 400 eV was applied in all calculations. The screened on-site Coulomb interaction $U$ and exchange interaction $J$ for Mn were set to 4.80 and 0.80 eV, respectively, based on previous literature estimates.[31] In these calculations, SOC was included on top of

the Schrödinger Hamiltonian and the direction of the Néel vector was set along [1$\bar{1}$00] direction, in accordance with experimental evidence from neutron diffraction and magneto-transport measurements.[21] As detailed in Note S2 and Figure S3, Supporting Information, it was observed that the band structure varied only slightly from one domain to another, enabling the main features of the bands to remain clearly visible in the experiments. In this case, it was assumed that the electronic structure along the ΓK and ΓM directions was equivalent to that along the $\Gamma K_3$ and $\Gamma M_2$ directions, respectively.

*DLM Combined with the CPA*: Self-consistent calculations were carried out using the fully relativistic Korringa-Kohn-Rostoker (SPRKKR) Green's function method in the atomic sphere approximation, within the rotationally invariant GGA+*U* scheme as implemented in the SPRKKR formalism.[32,33] The screened on-site Coulomb interaction *U* and exchange interaction *J* of Mn were set to 4.80 and 0.80 eV respectively, which were estimated based on the previous literature.[31] The angular momentum expansion up to *Imax* = 4 has been used for each atom on a 28 × 28 × 15 k-point grid. To simulate the paramagnetic phase, the DLM approach was employed, assigning an equal 50% probability to either sign for the magnetic orientation of antiparallel Mn atoms at $T \geq T_N$. The total energy convergence has been set to 10−5 Ry. The Lloyd's formula has been employed for accurate determination of the Fermi level.[34–36]

## Supporting Information

Supporting Information is available from the Wiley Online Library or from the author.

## Acknowledgements

M.H. and G.S. acknowledge the support by the Austrian Science Fund Grants P30960-N27 and I-4493-N as well as the JKU-Linz Grant LIT-2022-11-SEE-131. L.S. acknowledges support from JGU TopDyn initiative and Deutsche Forschungsgemeinschaft (DFG, German Research Foundation)—TRR 288—422213477 (projects A09 and B05). S.W.D., O.C., and J.M. thank QM4ST project financed by the Ministry of Education of Czech Republic, grant no. CZ.02.01.01/00/22_008/0004572, co-funded by the ERD. D.K. acknowledges the support from the Czech Academy of Sciences (project No. LQ100102201) and Czech Science Foundation; grant no. 22-22000M. J.M. acknowledges Czech NanoLab Research Infrastructure supported by MEYS CR (LM2023051). J.S.-B. acknowledges financial support from the Impuls- und Vernetzungsfonds der Helmholtz-Gemeinschaft under grant no. HRSF-0067. A.M. acknowledges the Czech Science Foundation grant no. 23-04746S. M.C. acknowledges financial support by the Deutsche Forschungsgemeinschaft through the International Collaborative Research Centre 160 (project nos. B8 and Z4) and the European Union's Horizon 2020 Research and Innovation Programme under Project SINFONIA; grant 964396. The ARPES setup was developed under the provision of the Polish Ministry and Higher Education project support for research and development with the use of research infrastructure of the National Synchrotron Radiation Centre "SOLARIS" under contract nr 1/SOL/2021/2. T.J acknowledges ERC Advanced Grant no. 101095925 and Ministry of Education of the Czech Republic Grant no. CZ.02.01.01/00/22008/0004594. T.J acknowledges ERC Advanced Grant no. 101095925 and Ministry of Education of the Czech Republic Grant no. CZ.02.01.01/00/22008/0004594.

## Conflict of Interest

The authors declare no conflict of interest.

## Author Contributions

M.H. and G.S. fabricated and characterized the samples, performed the UV-ARPES measurements, and analyzed the ARPES data. M.H. performed the GGA+*U* DFT calculations and S.W.D. and J.M. the DLM-CPA calculations. L.S. and T.J. discussed the physics of the altermagnetism and performed the spin-polarized bulk calculations. J.S.-B. participated in the UV-ARPES measurements at BESSY II, and G.K., T.Z., and N.O. participated in the UV-ARPES measurements at SOLARIS. O.C. and J.M. performed the STEM and D.K. the SQUID measurements. All authors discussed the ARPES data and its interpretations. G.S. conceived and supervised the project. M.H. wrote the manuscript with input from all authors.

## Data Availability Statement

The data that support the findings of this study are available from the corresponding author upon reasonable request.

## Keywords

altermagnetism, angle-resolved photoemission spectroscopy, electronic band structure, spintronics

Received: December 22, 2023
Revised: March 7, 2024
Published online: May 29, 2024

[1] I. Žutić, J. Fabian, S. D. Sarma, *Rev. Mod. Phys.* **2004**, *76*, 323.
[2] T. Jungwirth, X. Marti, P. Wadley, J. Wunderlich, *Nat. Nanotechnol.* **2016**, *11*, 231.
[3] V. Baltz, A. Manchon, M. Tsoi, T. Moriyama, T. Ono, Y. Tserkovnyak, *Rev. Mod. Phys.* **2018**, *90*, 15005.
[4] T. Jungwirth, J. Sinova, A. Manchon, X. Marti, J. Wunderlich, C. Felser, *Nat. Phys.* **2018**, *14*, 200.
[5] J. Železný, P. Wadley, K. Olejník, A. Hoffmann, H. Ohno, *Nat. Phys.* **2018**, *14*, 220.
[6] L. Šmejkal, J. Sinova, T. Jungwirth, *Phys. Rev. X.* **2022**, *12*, 011028.
[7] L. Šmejkal, R. González-Hernández, R. González-Hernández, T. Jungwirth, T. Jungwirth, J. Sinova, J. Sinova, *Sci. Adv.* **2020**, *6*, 23.
[8] S. Hayami, Y. Yanagi, H. Kusunose, *J. Phys. Soc. Japan* **2019**, *88*, 123702.
[9] L. D. Yuan, Z. Wang, J. W. Luo, E. I. Rashba, A. Zunger, *Phys. Rev. B* **2020**, *102*, 14422.
[10] R. González-Hernández, Š. Libor, K. Výborný, Y. Yahagi, J. Sinova, T. Jungwirth, Ž. Jakub, *Phys. Rev. Lett.* **2021**, *126*, 127701.
[11] I. I. Mazin, K. Koepernik, M. D. Johannes, R. González-Hernández, L. Šmejkal, *Proc. Natl. Acad. Sci. USA* **2021**, *118*, 1.
[12] L. Šmejkal, J. Sinova, T. Jungwirth, *Phys. Rev. X.* **2022**, *12*, 040501.
[13] R. D. Gonzalez Betancourt, J. Zubáč, R. Gonzalez-Hernandez, K. Geishendorf, Z. Šobáň, G. Springholz, K. Olejník, L. Šmejkal, J. Sinova, T. Jungwirth, S. T. B. Goennenwein, A. Thomas, H. Reichlová, J. Železný, D. Kriegner, *Phys. Rev. Lett.* **2023**, *130*, 036702.
[14] J. Krempaský, L. Šmejkal, S. W. D'Souza, M. Hajlaoui, G. Springholz, K. Uhlířová, F. Alarab, P. C. Constantinou, V. Strocov, D. Usanov, W. R. Pudelko, R. González-Hernández, A. Birk Hellenes, Z. Jansa, H. Reichlová, Z. Šobáň, R. D. Gonzalez Betancourt, P. Wadley, J. Sinova, D. Kriegner, J. Minár, J. H. Dil, T. Jungwirth, *Nature* **2024**, *626*, 517.
[15] J. D. Wasscher, *Solid State Commun.* **1965**, *3*, 169.
[16] S. Lee, S. Lee, S. Jung, J. Jung, D. Kim, Y. Lee, B. Seok, J. Kim, B. G. Park, L. Šmejkal, C.-J. Kang, C. Kim, *Phys. Rev. Lett.* **2023**, *132*, 036702.
[17] T. Osumi, S. Souma, T. Aoyama, K. Yamauchi, A. Honma, K. Nakayama, T. Takahashi, K. Ohgushi, T. Sato, *Phys. Rev. B* **2024**, *109*, 115102.
[18] O. Fedchenko, J. Minár, A. Akashdeep, S. W. D'Souza, D. Vasilyev, O. Tkach, L. Odenbreit, Q. Nguyen, D. Kutnyakhov, N. Wind, L.

Wenthaus, M. Scholz, K. Rossnagel, M. Hoesch, M. Aeschlimann, B. Stadtmüller, M. Kläui, G. Schönhense, T. Jungwirth, A. B. Hellenes, G. Jakob, L. Šmejkal, J. Sinova, H. J. Elmers, *Sci. Adv.* **2024**, *10*, 1.
[19] S. Reimers, L. Odenbreit, L. Smejkal, V. N. Strocov, P. Constantinou, A. B. Hellenes, R. J. Ubiergo, W. H. Campos, V. K. Bharadwaj, A. Chakraborty, T. Denneulin, W. Shi, R. E. Dunin-Borkowski, S. Das, M. Kläui, J. Sinova, M. Jourdan, *Nat. Commun.* **2024**, *15*, 2116.
[20] D. Kriegner, K. Výborný, K. Olejník, H. Reichlová, V. Novák, X. Marti, J. Gazquez, V. Saidl, P. Němec, V. V. Volobuev, G. Springholz, V. Holý, T. Jungwirth, *Nat. Commun.* **2016**, *7*, 11623.
[21] D. Kriegner, H. Reichlova, J. Grenzer, W. Schmidt, E. Ressouche, J. Godinho, T. Wagner, S. Y. Martin, A. B. Shick, V. V. Volobuev, G. Springholz, V. Holý, J. Wunderlich, T. Jungwirth, K. Výborný, *Phys. Rev. B* **2017**, *96*, 214418.
[22] D. Bossini, M. Terschanski, F. Mertens, G. Springholz, A. Bonanni, G. S. Uhrig, M. Cinchetti, *New J. Phys.* **2020**, *22*, 083029.
[23] D. Bossini, S. Dal Conte, M. Terschanski, G. Springholz, A. Bonanni, K. Deltenre, F. Anders, G. S. Uhrig, G. Cerullo, M. Cinchetti, *Phys. Rev. B* **2021**, *104*, 224424.
[24] P. E. Faria Junior, K. A. De Mare, K. Zollner, K. H. Ahn, S. I. Erlingsson, M. Van Schilfgaarde, K. Výborný, *Phys. Rev. B* **2023**, *107*, L100417.
[25] G. Yin, J. X. Yu, Y. Liu, R. K. Lake, J. Zang, K. L. Wang, *Phys. Rev. Lett.* **2019**, *122*, 106602.
[26] K. P. Kluczyk, K. Gas, M. J. Grzybowski, P. Skupiński, M. A. Borysiewicz, T. Fąs, J. Suffczyński, J. Z. Domagala, K. Grasza, A. Mycielski, M. Baj, K. H. Ahn, K. Výborný, M. Sawicki, M. Gryglas-Borysiewicz, *arXiv:2310.09134* **2023**.
[27] T. Komatsubara, M. Murakami, E. Hirahara, *J. Phys. Soc. Japan* **1963**, *18*, 356.
[28] P. E. Blöchl, *Phys. Rev. B* **1994**, *50*, 17953.
[29] G. Kresse, J. Furthmüller, *Comput. Mater. Sci.* **1996**, *6*, 15.
[30] J. P. Perdew, K. Burke, M. Ernzerhof, *Phys. Rev. Lett.* **1996**, *77*, 3865.
[31] S. Mu, R. P. Hermann, S. Gorsse, H. Zhao, M. E. Manley, R. S. Fishman, L. Lindsay, *Phys. Rev. Mater.* **2019**, *3*, 025403.
[32] H. Ebert, A. Perlov, S. Mankovsky, *Solid State Commun.* **2003**, *127*, 443.
[33] H. Ebert, D. Ködderitzsch, J. Minár, *Rep. Prog. Phys.* **2011**, *74*, 096501.
[34] P. Lloyd, *Proc. Phys. Soc.* **1967**, *90*, 217.
[35] P. Lloyd, P. V. Smith, *Adv. Phys.* **1972**, *21*, 69.
[36] R. Zeller, *J. Phys.: Condens.Matter* **2007**, *20*, 035220.